

InSight/MarCO Opportunistic Multiple Spacecraft Per Antenna (OMSPA) Demonstration

Andre Tkacenko*, Zaid Towfic*, Murphy C. Stratton**, Douglas S. Abraham*, Susan G. Finley*,
Shan Malhotra*, Andrew O'Dea*, Benjamin Kevin Malphrus**, Charles D. Conner**

*Jet Propulsion Laboratory, California Institute of Technology, 4800 Oak Grove Dr., Pasadena, CA 91109

{Andre.Tkacenko, Zaid.J.Towfic, Douglas.S.Abraham, Susan.G.Finley, Shantanu.Malhotra, James.A.Odea}@jpl.nasa.gov

**Morehead State University, 150 University Blvd., Morehead, KY 40351

{mcstratton, b.malphrus, c.conner}@moreheadstate.edu

Abstract—As smallsats become increasingly capable, longer-lived, and have more secondary payload launch opportunities to beyond-GEO destinations, they are expected to play an increasing role in deep space science investigations. This expectation is borne out by several relatively recent NASA Science Mission Directorate solicitations regarding smallsat studies and small innovative missions. With the potential for these smallsats to substantially add to the number of spacecraft operating in deep space, we need to be thinking about ways to support communications with all of them without the huge expense of trying to build a commensurate number of deep space antennas. One approach to this challenge might involve making greater use of beam-sharing techniques that allow all the spacecraft within the beamwidth of a single ground antenna to simultaneously downlink to the antenna. One of these techniques, Opportunistic Multiple Spacecraft Per Antenna (OMSPA), may be particularly suited to smallsats. In the concept for this technique, smallsats within the scheduled ground antenna beam of some other spacecraft, make opportunistic use of that spacecraft's beam by transmitting "open-loop" to a recorder associated with the antenna. These transmissions get captured on the recorder and can be later retrieved, demodulated, and decoded so that the smallsats can recover their data – all without them having to schedule the antenna itself and compete with larger missions for antenna time. Widespread use of such a technique could lead to more efficient use of receiver antenna resources and result in a dramatic increase in downlink throughput. An opportunity to demonstrate the technique occurred in May 2018, when the Mars CubeSat One (MarCO) mission, consisting of two nanospacecraft (MarCO-A & B) launched alongside InSight, a NASA Mars lander mission. To demonstrate the capabilities of OMSPA for this launch window opportunity, X-band downlink telemetry was recorded for all three spacecraft (InSight, MarCO-A, and MarCO-B) at both the Deep Space Network (DSN), using its 34-m antennas, and at Morehead State University (MSU) using its 21-m antenna – with all of the involved antennas pointed at InSight. Open-loop recordings were collected at the DSN using wideband very long baseline science receivers and at MSU using Universal Software Radio Peripheral (USR) devices operated using GNU Radio. All the recordings were then processed at the Jet Propulsion Laboratory, California Institute of Technology (JPL) using an OMSPA Software Receiver, a signal processing/communications tool used to extract telemetry transfer frames from baseband samples. The results of extracting telemetry data from InSight/MarCO recordings collected by the DSN and at MSU are described in this article. In particular, details pertaining to the processing chain used by the OMSPA Software Receiver to demodulate the DSN and MSU recordings are presented, from carrier/symbol synchronization, to frame alignment using attached sync markers (ASMs), followed by error correction code decoding. Validation results with closed-loop data obtained by the DSN are also presented in order to highlight the viability of OMSPA for future multiple spacecraft demodulation opportunities.

Copyright 2018. California Institute of Technology. Government sponsorship acknowledged.

The research was carried out at the Jet Propulsion Laboratory, California Institute of Technology, under a contract with the National Aeronautics and Space Administration.

TABLE OF CONTENTS

1. INTRODUCTION.....	1
2. OMSPA CONCEPT	2
3. OMSPA SIGNAL PROCESSING SOFTWARE RECEIVER MODULE	3
4. INSIGHT/MARCO LAUNCH WINDOW DEMONSTRATION SETUP	7
5. DOWNLINK DEMODULATION OF INSIGHT/MARCO RECORDINGS WITH THE OMSPA SOFTWARE RECEIVER.....	8
6. VALIDATION OF INSIGHT/MARCO RECOVERED TRANSFER FRAMES AGAINST DSN RECORDS....	11
7. CONCLUSION	16
ACKNOWLEDGMENTS	16
REFERENCES	16
BIOGRAPHY	17

1. INTRODUCTION

As small satellites (smallsats), such as CubeSats, continue to mature in terms of capabilities and longevity, they are increasingly being considered for supporting larger main satellite missions being developed at the National Aeronautics and Space Administration (NASA). In particular, they are expected to play an increasing support role in deep space science mission investigations. This expectation has been borne out by several recent NASA Science Mission Directorate solicitations regarding smallsat studies and small innovative missions.

Along with the potential for these smallsats to substantially add to the number of spacecraft operating in deep space comes the challenge of supporting telemetry communications with all of them. One straightforward solution to this issue would be to build a commensurate number of deep space antennas, however the substantial cost incurred with such an approach renders it not viable. Another method to face and potentially overcome this challenge involves utilizing beam-sharing techniques that allow all the spacecraft within the beamwidth of a single ground antenna to simultaneously downlink to or uplink from the antenna.

One such technique, referred to as Opportunistic Multiple Spacecraft Per Antenna (OMSPA) [1], may be particularly suited to smallsats being used to support larger main satellite missions. In the concept for this approach, smallsats within the scheduled ground antenna beam of some other spacecraft, make opportunistic use of that spacecraft's antenna beam coverage by transmitting *open-loop* to a recorder associated with the antenna. Such transmissions get captured by the

recorder and can then be later retrieved, demodulated, and decoded so that the data from the smallsats can be recovered - all without them having to schedule the antenna itself and compete with larger missions for antenna tracking time. Widespread use of such a technique could lead to more efficient use of receiver antenna resources and result in a dramatic increase in downlink throughput.

An opportunity to demonstrate the OMSPA technique occurred in May 2018, when the Mars CubeSat One (MarCO) mission, consisting of two nanospacecraft (MarCO-A & B) launched alongside InSight, a NASA robotic lander mission designed to study the interior of the planet Mars. To demonstrate the capabilities of OMSPA for this launch window opportunity, X-band downlink telemetry was recorded for all three spacecraft (InSight, MarCO-A, and MarCO-B) at both the Deep Space Network (DSN), using its 34-m antennas, and at Morehead State University (MSU), using its 21-m antenna - with all involved antennas pointing at InSight. Open-loop recordings were collected at the DSN using wideband very long baseline science receiver (WVSR) units and at MSU using Universal Software Radio Peripheral (USRP) devices operated using GNU Radio.

The recordings collected at MSU, as well as several WVSR recordings obtained by the DSN, were processed at the Jet Propulsion Laboratory (JPL), California Institute of Technology, using a signal processing/digital communications tool developed in MATLAB [2], referred to as the OMSPA Software Receiver, or the OMSPA Signal Processing module. This receiver took in baseband samples from each recording and extracted the telemetry transfer frames contained within.

In this article, we elaborate on the results of using the OMSPA Software Receiver to demodulate X-band downlink telemetry data captured from InSight/MarCO during the launch window time frame. We start with an overview of the processing chain used by the OMSPA Software Receiver to demodulate baseband telemetry from sample data files, from carrier/symbol synchronization, to frame alignment using attached synchronization markers (ASMs) [3], followed by subsequent error correction code decoding. From there, we show some of the intermediate outputs from the OMSPA Software Receiver used for diagnostic purposes, applied to the InSight/MarCO launch window data, including power spectral density (PSD) plots, scatter plot outputs from the carrier phase and symbol timing recovery blocks, followed by ASM cross-correlation plots used to indicate frame synchronization. These are included to provide a visual assessment of the fidelity of the overall telemetry demodulation process.

Recovered telemetry transfer frames obtained from the MSU USRP and DSN WVSR sample files for the InSight/MarCO launch window are then validated against closed-loop data obtained by the DSN. In particular, we note that for all possible cyclic redundancy check (CRC) passing transfer frames for which there could be a match with the DSN records, there was agreement. These results serve to highlight the viability of OMSPA for future multiple spacecraft demodulation opportunities.

Finally, we touch on possible future directions to pursue for the OMSPA concept. This includes a potential pathway for infusion of OMSPA into the DSN. The purpose of this is to show how OMSPA could be implemented in the future, and how a smallsat customer could utilize the OMSPA concept to recover/transmit telemetry data for antenna tracks for which multiple spacecraft appear in-beam.

Outline

In Section 2, more in-depth details of the OMSPA concept are presented, including identifying multiple in-beam link opportunities, supporting multiple simultaneous recordings, and processing of telemetry data. Implementation aspects related to the OMSPA Software Receiver module used to process the telemetry signals are covered in Section 3. In Section 4, specifics concerning the OMSPA demonstration setup used to accommodate the InSight/MarCO launch window opportunity are presented, including the recording setup used at MSU and the subsequent signal processing carried out at JPL. The results of demodulating the X-band downlink telemetry recorded from the InSight/MarCO launch window data captures using the OMSPA Software Receiver are presented in Section 5. There, the various stages of demodulation are presented, from carrier/symbol synchronization, to frame alignment and decoding. In Section 6, the results of validating the transfer frames recovered from the InSight/MarCO OMSPA demonstration against those obtained through the DSN are presented. Finally, in Section 7, concluding remarks are made.

Notation

All notations are as in [4] and [5]. In particular, parentheses will be used to denote continuous-time signals, whereas subscripts will be used to denote discrete-time sequences. Thus, $x(t)$ would represent a continuous-time signal for $t \in \mathbb{R}$, while c_n would denote a discrete-time sequence for $n \in \mathbb{Z}$.

2. OMSPA CONCEPT

A visual overview of the OMSPA concept [1] is illustrated in Figure 1. In this setting, a spacecraft with a formally scheduled communications link is tracked by a ground station antenna. The pointing of this antenna is based upon an ephemeris file indicating the trajectory of this scheduled spacecraft.

Smallsats expected to be in the vicinity of the scheduled spacecraft can submit their ephemeris files to the ground station facility. If there are periods of time for which any of these smallsats appear in-beam relative to the gain pattern of the antenna tracking the scheduled spacecraft, and the smallsats are themselves transmitting, then we have a potential OMSPA opportunity.

Assuming that the bandwidths of the smallsats and scheduled spacecraft downlinks within an OMSPA opportunity are non-overlapping, then the telemetry signal from each spacecraft can be recorded without any interference from any other spacecraft. All such signals can be captured by a wideband digital recorder as shown in Figure 1. Once recorded in an open-loop fashion, each telemetry signal can be demodulated in software as was done for the InSight/MarCO launch window OMSPA opportunity mentioned above. Through a secure Internet site, a smallsat mission operations center (MOC) can then either be given access to the open-loop recording itself or to output products such as the telemetry transfer frames, one-way Doppler estimates, and a quality of service (QoS) report.

In determining whether or not a given spacecraft is a viable candidate for an OMSPA service, several factors must be taken into account, as follows:

1. start/end time of the spacecraft's downlink radio session

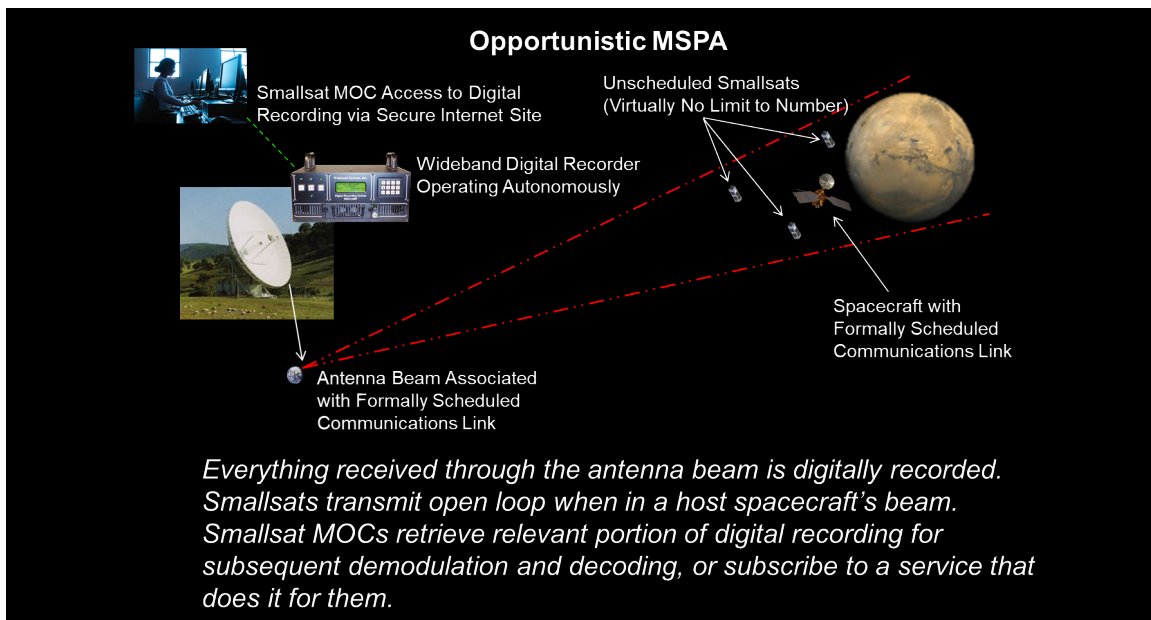


Figure 1. Visual overview of the general OMSPA concept.

- possibly including high gain antenna (HGA) / low gain antenna (LGA) attitude;
- 2. geometry of the spacecraft's trajectory to see if the spacecraft's downlink session is within the half-power beamwidth of the ground antenna;
- 3. sufficiency of the link budget - given the spacecraft effective isotropic radiated power (EIRP), range, and the ground antenna gain-to-noise-temperature (G/T);
- 4. compatibility of the spacecraft downlink polarization with the configuration of the ground antenna (some support simultaneous dual polarization, while others do not);
- 5. applicability of the ground track - the ground antenna is continuously pointing at the scheduled spacecraft over the course of the pass and not, for example, conducting very-long-baseline interferometry (VLBI) delta-differential one-way ranging (DDOR).

The beauty of the OMSPA concept approach comes from the fact that outside of bandwidth constraints, there is virtually no limit to the number of unscheduled smallsats whose telemetry can be recovered if they appear in-beam during a scheduled spacecraft track. Furthermore, outside of some computational resources required to identify OMSPA opportunities based on spacecraft ephemerides, as well as the availability of a wideband open-loop recorder, the overhead associated with supporting OMSPA is minimal. It is for these reasons that OMSPA is being considered for infusion into the DSN.

3. OMSPA SIGNAL PROCESSING SOFTWARE RECEIVER MODULE

Signal Model

Prior to introducing the OMSPA Signal Processing Software Receiver module, it is worthwhile considering the type of telemetry signals that will be encountered in this setting. For the vast majority of deep space type missions, pulse-coded modulation/phase-shift keyed/phase-modulated (PCM/PSK/PM) waveforms are used [6]. A model for the radio frequency (RF) received downlink PCM/PSK/PM sig-

nal $r_{\text{RF}}(t)$ is given below.

$$r_{\text{RF}}(t) = \sqrt{2\mathcal{P}_T} [d(t) \sin(mP(t)) \cos(2\pi (F_C + F_D) t + \theta_C) + \cos(mP(t)) \sin(2\pi (F_C + F_D) t + \theta_C)] + w(t). \quad (1)$$

Here, we have the following [6].

$$\begin{aligned} \mathcal{P}_T &\triangleq \text{transmit power,} \\ d(t) &\triangleq \text{data signal,} \\ m &\triangleq \text{modulation index,} \\ P(t) &\triangleq \text{subcarrier signal,} \\ F_C &\triangleq \text{carrier frequency,} \\ F_D &\triangleq \text{residual Doppler frequency,} \\ \theta_C &\triangleq \text{carrier phase,} \\ w(t) &\triangleq \text{noise process.} \end{aligned} \quad (2)$$

The data signal $d(t)$ contains the telemetry content of the downlink signal and can be expressed as follows.

$$d(t) \triangleq \sum_{k \in \mathcal{I}} d_k p(R_{\text{sym}} t - k - \epsilon), \quad (3)$$

where we have

$$\begin{aligned} d_k &\triangleq k\text{-th data constellation symbol,} \\ p(x) &\triangleq \text{data symbol pulse shape,} \\ R_{\text{sym}} &\triangleq \text{symbol rate,} \\ \epsilon &\triangleq \text{symbol timing offset (with } \epsilon \in [0, 1)), \\ \mathcal{I} &\triangleq \text{index set of active data symbols.} \end{aligned} \quad (4)$$

The data constellation symbol d_k can take on a number of values depending on the type of constellation used. Typically, for deep space applications, binary phase-shift keying

(BPSK) [4] is used, although quadrature phase-shift keying (QPSK) [4] is also sometimes employed. We have

$$d_k \in \begin{cases} \{-1, 1\}, & \text{for BPSK,} \\ \left\{ \left(\frac{1+j}{\sqrt{2}} \right), \left(\frac{-1+j}{\sqrt{2}} \right), \left(\frac{-1-j}{\sqrt{2}} \right), \left(\frac{1-j}{\sqrt{2}} \right) \right\}, & \text{for QPSK.} \end{cases}$$

For deep space applications, the pulse shape $p(x)$ from (4) appearing in (3) is typically either a non-return-to-zero (NRZ) [4] or bi-phase (Manchester) [4] type of pulse. These have the following representations [4].

NRZ:

$$p(x) \triangleq \begin{cases} 1, & -\frac{1}{2} \leq x < \frac{1}{2}, \\ 0, & \text{otherwise.} \end{cases}$$

bi-phase (Manchester):

$$p(x) \triangleq \begin{cases} 1, & -\frac{1}{2} \leq x < 0, \\ -1, & 0 \leq x < \frac{1}{2}, \\ 0, & \text{otherwise.} \end{cases}$$

The subcarrier signal $P(t)$ from (2) and (1) has the following form [6]:

$$P(t) \triangleq \begin{cases} 1, & \text{PCM/PM,} \\ \text{sqr}(2\pi F_{\text{SC}}t + \theta_{\text{SC}}), & \text{PCM/PSK/PM} \\ & \text{(square-wave),} \\ \sin(2\pi F_{\text{SC}}t + \theta_{\text{SC}}), & \text{PCM/PSK/PM} \\ & \text{(sine-wave).} \end{cases} \quad (5)$$

Here, we have the following.

$$\begin{aligned} F_{\text{SC}} &\triangleq \text{ subcarrier frequency,} \\ \theta_{\text{SC}} &\triangleq \text{ subcarrier phase,} \\ \text{sqr}(x) &\triangleq \text{ square-wave pulse.} \end{aligned}$$

The square-wave pulse is the rectified version of the sine-wave, which mathematically can be expressed as

$$\text{sqr}(x) = \text{sgn}(\sin(x)).$$

The noise process $w(t)$ from (2) and (1) is assumed to be a real additive white Gaussian noise (AWGN) [4] process with two-sided power spectral density (PSD) $\frac{N_0}{2}$.

Upon RF downconversion, the signal $r_{\text{RF}}(t)$ is converted to an intermediate frequency (IF) signal $r_{\text{IF}}(t)$, given by a low-pass filtered version of the quantity $r_{\text{RF}}(t)$ multiplied by $2 \cos(2\pi F_{\text{IF}}t)$, where F_{IF} is the IF downconversion frequency, used to bring the frequency content of the resulting signal as close to zero frequency as possible without any spectral overlap taking place [5]. Effectively, both the RF and IF signals correspond to a complex baseband (CB) [4] version $r_{\text{CB}}(t)$, which from (1), is given by

$$r_{\text{CB}}(t) = \sqrt{\mathcal{P}_T} \times [d(t) \sin(mP(t)) - j \cos(mP(t))] \times e^{j(2\pi F_{\text{D}}t + \theta_{\text{C}})} + v(t). \quad (6)$$

Here, $v(t)$ is a circularly-symmetric complex AWGN process [4] with PSD N_0 . Mathematically, the CB signal $r_{\text{CB}}(t)$

is obtained from the IF signal $r_{\text{IF}}(t)$ by multiplying by $\sqrt{2} \cos(2\pi (F_{\text{C}} - F_{\text{IF}})t)$ followed by low-pass filtering to obtain the real part, or in-phase (I) component, and multiplying by $-\sqrt{2} \sin(2\pi (F_{\text{C}} - F_{\text{IF}})t)$ followed by low-pass filtering to obtain the imaginary part, or quadrature (Q) component [4], [5]. With the IF signal $r_{\text{IF}}(t)$ further low-pass filtered for sampling at frequency F_s , effectively, the CB version of the signal is as in (6), but with $v(t)$ now being a circularly-symmetric complex Gaussian process with PSD $S_v(F)$ [5] given by

$$S_v(F) = \begin{cases} N_0, & -\frac{F_s}{2} \leq F < \frac{F_s}{2}, \\ 0, & \text{otherwise.} \end{cases} \quad (7)$$

With $r_{\text{CB}}(t)$ as in (6), where $v(t)$ has a PSD of x as in (7), the sequence of received samples r_n is given as

$$\begin{aligned} r_n &\triangleq r_{\text{CB}}\left(\frac{n}{F_s}\right), \\ &= \sqrt{\mathcal{P}_T} \times \\ &\quad \left[d\left(\frac{n}{F_s}\right) \sin\left(mP\left(\frac{n}{F_s}\right)\right) - j \cos\left(mP\left(\frac{n}{F_s}\right)\right) \right] \\ &\quad \times e^{j(2\pi f_{\text{D}}n + \theta_{\text{C}})} + v_n. \end{aligned} \quad (8)$$

Here, $f_{\text{D}} \triangleq \frac{F_{\text{D}}}{F_s}$ is the *normalized residual Doppler frequency*. Also, v_n is a circularly-symmetric complex AWGN sequence with variance $\sigma_v^2 = N_0 F_s$ [5]. From (3), the quantity $d\left(\frac{n}{F_s}\right)$ appearing in (8) can be expressed as follows:

$$d\left(\frac{n}{F_s}\right) = \sum_{k \in \mathcal{I}} d_k p\left(\frac{n}{O} - k - \epsilon\right),$$

where $O \triangleq \frac{F_s}{R_{\text{sym}}}$ is the *oversampling factor*, i.e., the number of samples per symbol. Similarly, from (5), the quantity $P\left(\frac{n}{F_s}\right)$ appearing in (8) can be expressed as

$$P\left(\frac{n}{F_s}\right) \triangleq \begin{cases} 1, & \text{PCM/PM,} \\ \text{sqr}(2\pi f_{\text{SC}}n + \theta_{\text{SC}}), & \text{PCM/PSK/PM} \\ & \text{(square-wave),} \\ \sin(2\pi f_{\text{SC}}n + \theta_{\text{SC}}), & \text{PCM/PSK/PM} \\ & \text{(sine-wave),} \end{cases}$$

where $f_{\text{SC}} \triangleq \frac{F_{\text{SC}}}{F_s}$ is the *normalized subcarrier frequency*.

The received sequence r_n from (8) is complex in general and nominally represents the input samples to the OMSPA Signal Processing Software Receiver. It admits the following decomposition:

$$r_n = r_{I,n} + jr_{Q,n},$$

where $r_{I,n} \triangleq \text{Re}[r_n]$ and $r_{Q,n} \triangleq \text{Im}[r_n]$ denote, respectively, the in-phase (I) and quadrature (Q) components of the baseband sequence r_n [4], [5].

OMSPA Software Receiver Module Details

A block diagram of the OMSPA Software Receiver module, which was implemented in MATLAB for this effort [2], is shown in Figure 2. As can be seen, the Software Receiver module consists of three main subsystems: carrier phase recovery, symbol timing recovery, and frame synchronization/decoding. Each of these subsystems successively transforms the input samples to output transfer frames.

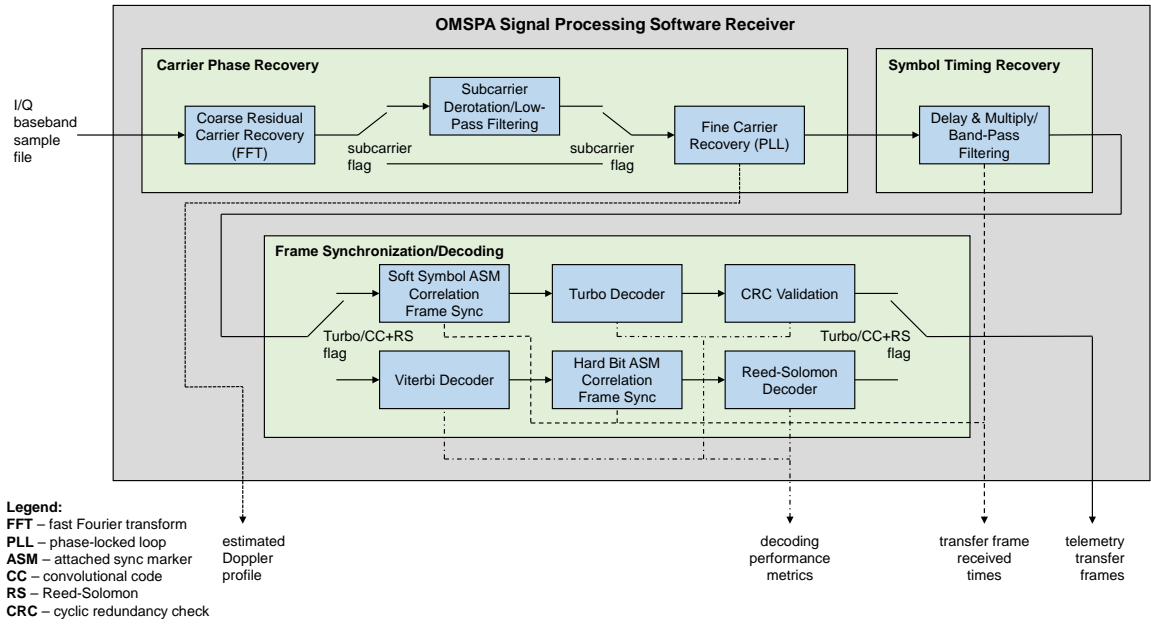


Figure 2. Block diagram of the OMSPA Signal Processing Software Receiver module.

Carrier Phase Recovery—The sequence of I/Q baseband samples r_n from (8) is input to the OMSPA Software Receiver and passed to the carrier phase recovery subsystem as shown in Figure 2. Roughly speaking, the purpose of the carrier phase recovery subsystem is to undo the phase term $e^{j(2\pi f_D + \theta_C)}$ present in the expression for r_n given in (8).

The first step towards undoing the phase consists of a coarse residual carrier correction which involves identifying the peak frequency value of the signal and translating this value to zero frequency. In other words, the first step involves finding the frequency f_0 which maximizes the absolute value of the discrete-time Fourier transform (DTFT) [5] of the sequence r_n , namely $R(e^{j2\pi f})$, and translating the DTFT by this value, resulting in the signal with DTFT $R(e^{j2\pi(f-f_0)})$.

Instead of explicitly calculating the DTFT for all frequencies f , samples of the DTFT are computed using the discrete Fourier transform (DFT) [5] with N_{DFT} points, yielding the DTFT at the frequency values $f_\ell = \frac{\ell}{N_{\text{DFT}}}$, where $\ell \in \{-\lfloor \frac{N_{\text{DFT}}}{2} \rfloor, \dots, \lfloor \frac{N_{\text{DFT}}}{2} \rfloor - 1\}$. When N_{DFT} is a power of 2, i.e., $N_{\text{DFT}} = 2^q$ for some $q \in \mathbb{N}$, the DFT can be computed in $\mathcal{O}(N_{\text{DFT}} \log_2 N_{\text{DFT}}) = \mathcal{O}(q2^q)$ complexity, using an algorithm known as the fast Fourier transform (FFT) [5]. This was used in the OMSPA Software Receiver to carry out the coarse residual carrier correction. From (8), at the output of the coarse correction stage, the resulting sequence $r_{\text{CPR}_{1,n}}$ is approximately

$$r_{\text{CPR}_{1,n}} = \sqrt{\mathcal{P}_T} \times \left[d\left(\frac{n}{F_s}\right) \sin\left(mP\left(\frac{n}{F_s}\right)\right) - j \cos\left(mP\left(\frac{n}{F_s}\right)\right) \right] \times e^{j\theta_C} + v_{\text{CPR}_{1,n}}, \quad (9)$$

where $v_{\text{CPR}_{1,n}}$ is a circularly-symmetric complex AWGN sequence with variance $N_0 F_s$.

After the bulk of the residual carrier or Doppler f_D from (8) has been removed, the next step involves extracting one of

the subcarrier images from the data, if a subcarrier is present. In the event that a subcarrier is present, the output from the coarse correction stage is frequency shifted by $\pm f_{\text{SC}}$, to shift either the left or right subcarrier image to baseband, and then low-pass filtered to remove any residual carrier components and subcarrier images, as shown in Figure 2. From (9), the output of this stage is effectively given by

$$r_{\text{CPR}_{2,n}} = \alpha \sqrt{\mathcal{P}_T} \left[d\left(\frac{n}{F_s}\right) \sin(m) \right] e^{j\theta_C} + v_{\text{CPR}_{2,n}}, \quad (10)$$

where α is a factor satisfying $\alpha \leq 1$ used to represent the fraction of signal energy contained in the subcarrier image and $v_{\text{CPR}_{2,n}}$ is a circularly-symmetric complex AWGN sequence with variance $N_0 F_s$. If no subcarrier is present, then the output of this stage is simply given by

$$r_{\text{CPR}_{2,n}} = \sqrt{\mathcal{P}_T} \left[d\left(\frac{n}{F_s}\right) \sin(m) - j \cos(m) \right] e^{j\theta_C} + v_{\text{CPR}_{2,n}}, \quad (11)$$

Finally, to remove the constant phase offset θ_C , along with any slowly changing residual phase trajectory still present in the sequence $r_{\text{CPR}_{2,n}}$, a fine carrier phase recovery is carried out using a phase-locked loop (PLL), as shown in Figure 2. The input to the PLL is given by the sequence $r_{\text{CPR}_{2,n}}$ raised to a particular power to remove the effects of the data and make the data and residual carrier line up in phase. Specifically, if BPSK is used, then $r_{\text{CPR}_{2,n}}$ is squared, whereas if QPSK is used, then $r_{\text{CPR}_{2,n}}$ is raised to the fourth power. The resulting auxiliary signal is then input to a second order PLL [5]. In order to account for PLL transient effects due to acquisition, the OMSPA Software Receiver can process a block of samples twice, first in forward order, and then in reverse, with the final output phase trajectory being that of the reverse pass, but itself reversed to correspond to the original time evolution orientation.

The PLL yields a sequence of residual Doppler phase estimates $\phi_n \triangleq e^{j\hat{\theta}_n}$, which can optionally be output from

the OMSPA Software Receiver to provide one-way Doppler estimates as shown in Figure 2. With the PLL output applied to the input sequence $r_{\text{CPR},n}$ given in either (10) or (11), the resulting output sequence $r_{\text{CPR},n}$ is approximately given by the following.

$$r_{\text{CPR},n} = \begin{cases} \beta\sqrt{\mathcal{P}_T}d\left(\frac{n}{F_s}\right) + v_{\text{CPR},n}, & \text{subcarrier present,} \\ \beta\sqrt{\mathcal{P}_T}\left[d\left(\frac{n}{F_s}\right) - j\cot(m)\right] + v_{\text{CPR},n}, & \text{subcarrier absent,} \end{cases} \quad (12)$$

where β is a factor satisfying $\beta = \alpha \sin(m)$ or $\beta = \sin(m)$ if a subcarrier is present or absent, respectively, and $v_{\text{CPR},n}$ is a circularly-symmetric complex AWGN sequence with variance $N_0 F_s$.

Symbol Timing Recovery—The purpose of the symbol timing recovery subsystem is to extract the sequence of symbols d_k from (3) from the input sample sequence $r_{\text{CPR},n}$ from (12). As shown in Figure 2, this is carried out via a delay & multiply / band-pass filtering approach [4], [5].

First, the sequence $r_{\text{CPR},n}$ from (12) is processed by the *matched filter* [4], [5] for the data signal $d(t)$ from (3). The impulse response of the matched filter is given by $p^*(-x)$ [5]. Pragmatically, given the sampled instances of the data signal $d\left(\frac{n}{F_s}\right)$ from (12), the matched filter $p^*(-x)$ is not implemented as a continuous-time convolution, but rather as a discrete-time convolution with the sampled matched filter sequence $p^*\left(-\frac{n}{O}\right)$ [5], where $O = \frac{F_s}{R_{\text{sym}}}$ is the oversampling factor. In other words, the following sequence is formed:

$$r_{\text{STR},n} = r_{\text{CPR},n} \otimes p^*\left(-\frac{n}{O}\right), \quad (13)$$

where the glyph \otimes denotes convolution [5].

From the matched filter output $r_{\text{STR},n}$ from (13), an auxiliary signal is formed by multiplying $r_{\text{STR},n}$ by a delayed, conjugated version of itself, and finally extracting the real part. The amount of delay depends upon the type of pulse shaping used. If an NRZ type pulse shape is used, then the delay amount is $\frac{O}{2}$, whereas if a bi-phase pulse shape is employed, then the amount of delay is $\frac{O}{4}$. This then leads to the following auxiliary signal:

$$r_{\text{STR}_{\text{aux}},n} = \begin{cases} \text{Re}\left[r_{\text{STR},n}r_{\text{STR},n-\frac{O}{2}}^*\right], & \text{NRZ,} \\ \text{Re}\left[r_{\text{STR},n}r_{\text{STR},n-\frac{O}{4}}^*\right], & \text{bi-phase.} \end{cases} \quad (14)$$

It should be noted that the auxiliary sequence $r_{\text{STR}_{\text{aux}},n}$ from (14), sometimes called the timing wave, is used for symbol synchronization.

The key to synchronizing with respect to the symbols comes from the fact that the timing wave $r_{\text{STR}_{\text{aux}},n}$ from (14) should have a harmonic at twice the baud or symbol rate, which occurs at $f_H \triangleq \frac{2}{O}$ in the sampled discrete-time frequency domain. In the OMSPA Software Receiver, this harmonic is isolated using a discrete-time band-pass filter centered at frequency f_H .

With the timing wave $r_{\text{STR}_{\text{aux}},n}$ band-pass filtered around f_H , the zero-crossings of the output sequence represent the symbol synchronized timing instances. These timing instances

are used to resample the matched filter output $r_{\text{STR},n}$ from (13). The resulting output from the symbol timing recovery subsystem is thus effectively

$$r_{\text{STR},k} = d_k + v_{\text{STR},k}, \quad (15)$$

where $v_{\text{STR},k}$ is a circularly-symmetric complex AWGN sequence with variance $\sigma_{v_{\text{STR}}}^2 = \frac{1}{\rho}$, where ρ is the signal-to-noise ratio (SNR) [4], [5] given by $\rho = \frac{\beta^2 \mathcal{P}_T}{N_0 R_{\text{sym}}}$.

Frame Synchronization/Decoding—With the symbol stream $r_{\text{STR},k}$ from (15) output from the OMSPA Software Receiver symbol timing recovery subsystem, the final step required before transfer frames are yielded consists of synchronizing to each frame boundary and performing decoding to correct any errors in transmission. As shown in Figure 2, this is carried out in one of two ways depending on the type of coding used.

For all spacecraft downlink telemetry of interest, data is arranged in transfer frame (TF) units that are constructed and encoded according to the Consultative Committee for Space Data Systems (CCSDS) standard [7], [3]. For a typical deep space mission, the TFs are encoded using either a turbo code or a convolutional code (CC) inner code / Reed-Solomon (RS) outer code type combination (commonly dubbed CC+RS) [7]. The TFs are assembled differently depending upon whether turbo or CC+RS encoding is used.

In particular, the main difference between the way the TFs are constructed involves how the frame synchronization pattern is inserted into the data stream. Here, frame sync is carried out using an attached synchronization marker (ASM) [7], [3], which is a known bit pattern that prepends a TF after it has undergone one layer of encoding. This is illustrated in Figure 3, which shows how the CCSDS TFs are structured for (a) turbo encoded data and (b) CC+RS encoded data. (Typically, after one layer of encoding has been performed, the resulting bit stream is also randomized, using a known pseudo-randomization scheme [7], [3].)

The TF boundaries can be identified by exploiting the known ASM sequence. Specifically, the TF boundaries can be determined by correlating the received TF sequence with the ASM. However, this requires that the ASM appears in a meaningful form in the resultant sequence. As can be seen in Figure 3, for turbo encoded data, the ASM appears as is in the output bit stream, whereas for CC+RS encoded data, the ASM is hidden behind a layer of convolutional coding. It is for this reason that for the OMSPA Software Receiver, frame synchronization is handled differently depending upon whether turbo or CC+RS coding has been used.

From Figure 2, it can be seen that for the OMSPA Software Receiver frame synchronization/decoding subsystem that one of two methods is used for frame sync, depending on the type of encoding which has been applied. Recall that the input to the OMSPA Software Receiver frame synchronization/decoding subsystem is $r_{\text{STR},k}$ from (15), which is essentially the sequence of soft symbols. For turbo encoded data, the ASM should be present in this stream as is, and so for this case, the TF boundaries can be determined by correlating the soft symbol sequence $r_{\text{STR},k}$ with the ASM sequence. On the other hand, for CC+RS encoded data, the CC outer code must first be stripped off before any correlation with the ASM can be made. This is carried out using a Viterbi decoder [4], in which a node sync algorithm, such as that used in the Electra radio [8], is employed in the OMSPA Software Receiver to

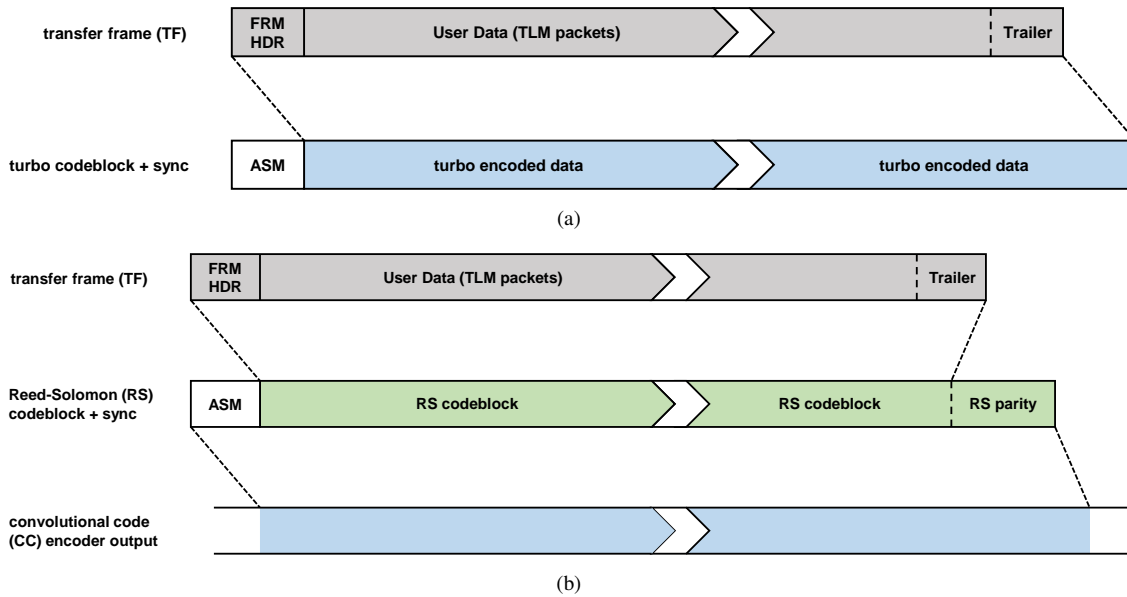


Figure 3. CCSDS transfer frame (TF) structure for (a) turbo encoded data and (b) convolutional code (CC) + Reed-Solomon (RS) encoded data. (FRM: frame, HDR: header, TLM: telemetry, ASM: attached sync marker.)

properly determine the delay of the CC. The output of the Viterbi decoder is a stream of hard decision bits [4]. This hard bit stream is then correlated with the ASM sequence, as shown in Figure 2.

In addition to helping determine the TF boundary locations, the ASM correlation blocks from Figure 2 can be used to provide TF received timing information, when combined with the symbol timing instances output from the OMSPA Software Receiver symbol timing recovery subsystem. This can be used to output Earth Received Time (ERT) values for each TF, which are typically reported according to the 0161-Telecomm Telemetry Standard Formatted Data Unit (SFDU) Interface [9].

After frame synchronization has been accomplished through correlation with the ASM sequence, de-randomization is carried out if necessary, followed by decoding of the turbo code, for turbo encoded data, or decoding of the RS outer code, for CC+RS encoded data. For turbo encoded data, each TF consists of a cyclic redundancy check (CRC) code in the trailer (see Figure 3), which can be used to faithfully detect whether or not the TF is in error. This is the role of the CRC validation block shown in Figure 2, which compares the received CRC bits at the trailer of a given TF with the CRC calculated from the user data bits of the TF. If all received/calculated CRC bits match, then the TF is deemed valid, whereas if not, then the TF is considered to be erroneous.

The main output of the OMSPA Software Receiver frame synchronization/decoding subsystem consists of the extracted telemetry TFs. In addition, the output of all of the decoder blocks (i.e., the turbo and CRC decoders for turbo encoded data and the Viterbi and RS decoders for CC+RS encoded data) includes performance metrics which can be used as a diagnostic to assess the quality or fidelity of the decoding process.

4. INSIGHT/MARCO LAUNCH WINDOW DEMONSTRATION SETUP

On May 5th, 2018, at 11:05 Universal Time Coordinated (UTC), both InSight and the two Mars CubeSat One (MarCO) nanosatellites (MarCO-A & MarCO-B), were launched from the Atlas V 401 rocket from Vandenberg Air Force Base SLC-3E. For this launch window, MarCO-A and MarCO-B appeared in-beam from a typical deep space antenna aiming at InSight. To test the OMSPA Software Receiver for this opportunity, downlink telemetry from the three spacecraft were recorded at Morehead State University (MSU) during this launch window.

A 21-m space tracking antenna at the Space Science Center at MSU (see Figure 4) was used to track and capture X-band downlink telemetry from InSight, MarCO-A, and MarCO-B. In particular, ephemeris data for InSight provided by the Jet Propulsion Laboratory (JPL), California Institute of Technology, was supplied to MSU and used to orient the antenna.

With the 21-m antenna locked on to the InSight trajectory, X-band downlink telemetry from each of the spacecraft was recorded, as shown in Figure 5. This was done by splitting the received signal from the antenna into three parallel paths, and downconverting each radio frequency (RF) signal down to intermediate frequency (IF) [5]. The carrier frequencies for the X-band downlink telemetry for each of the spacecraft were as follows:

- InSight: $F_C = F_{C;NSYT}$,
- MarCO-A: $F_C = F_{C;MCOA}$,
- MarCO-B: $F_C = F_{C;MCOB}$.

After downconversion to IF, each resulting signal was converted to complex baseband (CB) and sampled. This was carried out using Universal Software Radio Peripheral (USRP) devices connected to desktop computers running GNU Radio. As the processing power of these desktop computers was limited to Intel® Core™ 2 Duo microprocessors, each downlink



Figure 4. MSU Space Science Center 21-m antenna.

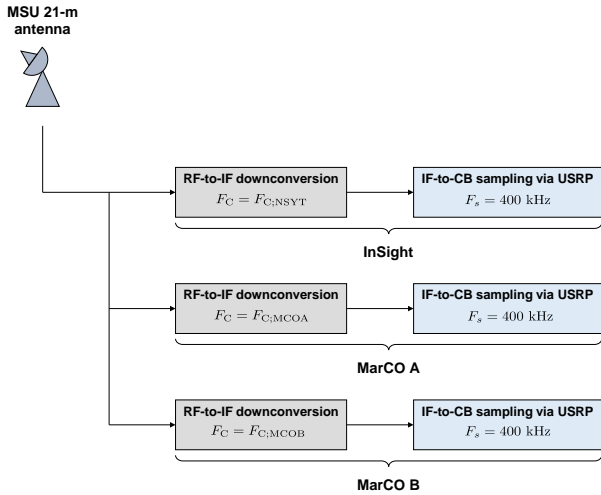


Figure 5. MSU InSight/MarCO OMPSA launch window opportunity data capture setup.

telemetry signal was sampled at 400 kHz, as shown in Figure 5.

This sampling rate of 400 kHz was deemed sufficient to properly capture the downlink telemetry from each spacecraft, given the telemetry parameters used during the launch window. The one caveat to this was for capturing InSight data, given its relatively large subcarrier frequency. For the InSight data captures, the IF-to-CB downconversion was deliberately offset by 121.25 kHz, in order to capture both the residual carrier, along with one of the subcarrier data images (see Section 5 for more details).

Telemetry was captured over the launch window from May

	InSight	MarCO-A	MarCO-B
DOY 126	Green	Green	Green
DOY 127	Red	Green	Yellow
DOY 128	Red	Green	Green

Legend:

- – data erroneously captured,
- – data not captured,
- – data correctly captured.

Table 1. Assessment of MSU sample data record fidelity from InSight/MarCO launch window.

6-8, 2018 (day-of-year (DOY) 126, 127, and 128). However, due to various recording issues, meaningful sample data was only captured for a certain subset of these days for each spacecraft. An assessment of the fidelity of the data records captured by MSU for the InSight/MarCO launch window is shown in Table 1. Specifically, for InSight, on DOY 127 and 128, telemetry was only captured for a small window of time, and with an incorrect setting of the carrier frequency offset to capture any telemetry data from the subcarrier images. For MarCO-B, data was simply not captured during DOY 127.

5. DOWNLINK DEMODULATION OF INSIGHT/MARCO RECORDINGS WITH THE OMPA SOFTWARE RECEIVER

Sample X-band downlink telemetry data files from the InSight/MarCO launch window that were captured at MSU were then sent over to JPL for demodulation processing using the OMPA Software Receiver. Nominal telemetry settings used by InSight, MarCO-A, and MarCO-B during this launch window are shown in Table 2. A brief description of the demodulation results for each data capture is described below.

InSight DOY 126 Demodulation Results

A recording of X-band downlink telemetry from InSight on DOY 126 was captured from MSU over the following approximate epoch:

- Start time: 2018, DOY 126, 09:00:00 UTC,
- End time: 2018, DOY 126, 10:40:00 UTC.

As mentioned previously in Section 4 and shown in Figure 5, the sample rate used to sample the received CB signal was 400 kHz. As this sample rate was insufficient to capture both the residual carrier and one set of left/right subcarrier images, the carrier frequency was deliberately offset by approximately 121.25 kHz in order to recover both the residual carrier as well as one of the subcarrier images. In this case, the left subcarrier image was preserved by using this approach.

Plots of intermediary quantities generated with the OMPA Software Receiver for this InSight pass are shown in Figure 6. In particular, the input sample PSD, the evolution of the recovered signal from samples to symbols, and the result of the cross-correlation of the Viterbi decoder output with the ASM sequence are shown in Figure 6(a), (b), and (c),

	InSight	MarCO-A	MarCO-B
modulation type	PCM/PSK/PM; NRZ-L BPSK	PCM/PSK/PM; NRZ-L BPSK	PCM/PSK/PM; NRZ-L BPSK
subcarrier	yes	yes	yes
coding	CC+RS	turbo	turbo
ASM bit pattern	1ACFFC1D	25D5C0CE8990F6C9461BF79C DA2A3F31766F0936B9E40863	25D5C0CE8990F6C9461BF79C DA2A3F31766F0936B9E40863
TF length	10232	8920	8920

Table 2. Nominal telemetry settings for X-band downlink used by InSight/MarCO spacecraft during launch window.

respectively.

As can be seen from Figure 6(a), the residual carrier can be seen to be located at approximately 121.25 kHz, and the left subcarrier image can be seen to be located at approximately -160 kHz. Furthermore, it can be seen that this choice of carrier frequency offset allowed for a sufficient number of NRZ side lobes [5] from the subcarrier image to be captured with the 400 kHz sample rate.

From Figure 6(b), the evolution of the received signal from samples to symbols through the use of the Carrier Phase Recovery and Symbol Timing Recovery subsystems of the OMSPA Software Receiver is evident. From the amorphous set of input samples, the underlying BPSK constellation can be seen at the output of the Carrier Phase Recovery subsystem. After this subsystem, only the real parts of the signal are preserved and used to find the proper symbol center values via the Symbol Timing Recovery subsystem. As can be seen, at the output of this latter subsystem, distinct BPSK symbols can be discerned, with no transitional values present near the vertical line at the origin.

The extracted symbols are then passed to the Frame Synchronization/Decoding subsystem. As the InSight downlink TFs were constructed using a CC+RS based encoding, the symbols were first passed to a Viterbi decoder to remove the CC inner code. To obtain the proper delay value for the CC, a node sync algorithm [8] was used. The output of the Viterbi decoder, which consisted of a stream of hard bit decisions, was then correlated with the ASM sequence to find the boundaries of the TFs. This is shown in Figure 6(c), where each of the local peaks, denoted with a red circle, indicate the beginning of one TF. As the ASM for the InSight pass is the 32-bit sequence described in Table 2 (i.e., 1ACFFC1D in hexadecimal), the maximum possible correlation value that can be achieved is 32, (assuming that a 0 is mapped to a -1 value and a 1 is mapped to a 1 value). From Figure 6(c), it can be seen that the maximum possible correlation value of 32 was obtained for each possible frame boundary, as the signal fidelity in this case was strong and the Viterbi decoder outputted no decoding errors.

Over the course of the 100 minute pass, a total of 2805 TFs, for which no decoding errors were reported, was recovered from the InSight DOY 126 pass.

MarCO-A DOY 126, 127, 128 Demodulation Results

X-band downlink telemetry from MarCO-A on DOY 126, 127, and 128 was captured from MSU over the following approximate epochs:

- DOY 126:
 - Start time: 2018, DOY 126, 08:47:25 UTC,
 - End time: 2018, DOY 126, 09:16:27 UTC;
- DOY 127:
 - Start time: 2018, DOY 127, 09:30:56 UTC,
 - End time: 2018, DOY 127, 09:51:29 UTC;
- DOY 128:
 - Start time: 2018, DOY 128, 13:06:11 UTC,
 - End time: 2018, DOY 128, 13:34:45 UTC.

Plots of intermediary quantities generated with the OMSPA Software Receiver for the MarCO-A DOY 126 pass are shown in Figure 7. In particular, the input sample PSD, the evolution of the recovered signal from samples to symbols, the result of the cross-correlation of the output soft symbols with the ASM sequence, and the ASM/data symbols for one identified TF block are shown in Figure 7(a), (b), (c), and (d), respectively.

As can be seen from Figure 7(a), the residual carrier is close to zero frequency, but offset by some amount on account of the relative Doppler seen from MarCO-A when tracking InSight. Unlike the case for InSight, the sample rate of 400 kHz is sufficient to capture both the residual carrier as well as several subcarrier images.

From Figure 7(b), it can be seen that the evolution of the received signal from samples to symbols through the use of the Carrier Phase Recovery and Symbol Timing Recovery subsystems of the OMSPA Software Receiver is similar to that seen for InSight. At the output of the Symbol Timing Recovery subsystem, noticeably distinct BPSK symbols can be discerned.

These symbols are then processed by the Frame Synchronization/Decoding subsystem. As the MarCO downlink TFs are formed using a turbo based encoding, the soft symbols are first correlated with the ASM sequence to align to the frame boundaries. This can be seen in Figure 7(c), in which each of the local peaks, marked with a red circle, indicate the beginning of one frame. The distinctly perceptible peaks relative to the other levels of the cross-correlation suggest that frame synchronization is correctly identifying the frame boundaries.

In Figure 7(d), the ASM and data symbols for one synchronized frame block are shown. The upper panel shows the ASM soft symbols (received waveform) plotted alongside the ASM sequence (template waveform), in order to highlight the agreement between the two. In the lower panel, the data symbols are plotted, effectively showing the time series of slightly noisy BPSK symbols.

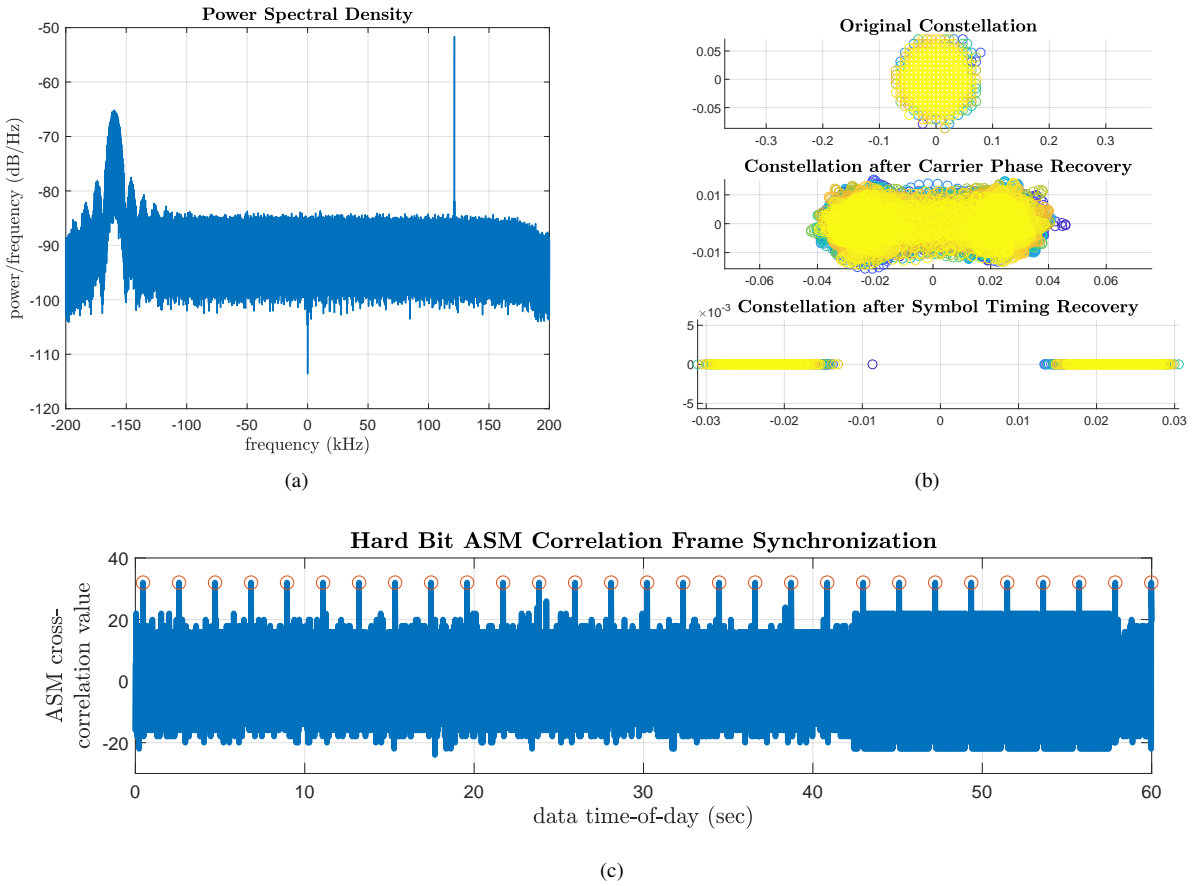


Figure 6. InSight DOY 126 downlink demodulation result using the OMSPA Software Receiver: (a) input sample PSD, (b) evolution from samples to symbols via the Carrier Phase/Symbol Timing Recovery subsystems, (c) hard bit cross-correlation of Viterbi decoder output with ASM sequence.

As shown in Figure 2, after frame synchronization has been carried out, the resulting frames are applied to a turbo decoder to recover the TFs. With the TFs extracted, a CRC is calculated for each TF (also shown in Figure 2), in order to more definitively ascertain whether or not the TF has been recovered error free.

Similar demodulation results (not shown here) were found for the MarCO-A DOY 127 pass. To show the effects of the expected decrease in SNR as the spacecraft moved farther away from the Earth, demodulation results with the OMSPA Software Receiver for the MarCO-A DOY 128 pass are shown in Figure 8. There, the effects of a smaller SNR are clearly evident. In particular, the power from the subcarrier images is lower (compare Figure 8(a) with Figure 7(a)), the soft BPSK symbols are more noisy (compare Figure 8(b) and (d) with Figure 7(b) and (d)), and the correlation peaks with the ASM are slightly lower (compare Figure 8(c) with Figure 7(c)).

Over the course of the MarCO-A passes, the following results were found:

- DOY 126: 187 TFs recovered, all passed CRC,
- DOY 127: 135 TFs recovered, all passed CRC except for one TF (the 5th one),
- DOY 128: 187 TFs recovered, all passed CRC except for 15 TFs.

MarCO-B DOY 126, 128 Demodulation Results

X-band downlink telemetry from MarCO-B on DOY 126, and 128 was captured from MSU over the following approximate epochs:

- DOY 126:
 - Start time: 2018, DOY 126, 10:19:53 UTC,
 - End time: 2018, DOY 126, 10:40:19 UTC;
- DOY 128:
 - Start time: 2018, DOY 128, 12:42:35 UTC,
 - End time: 2018, DOY 128, 13:11:09 UTC.

Demodulation results for the MarCO-B DOY 126 pass were similar to those for the MarCO-A DOY 126 pass, and as such, have not been plotted here. For DOY 128, however, an unusual phenomenon occurred which needed to be manually accommodated through separate applications of the OMSPA Software Receiver. During the course of the DOY 128 pass, MarCO-B switched telemetry modes from the nominal lower rate configuration described in Table 2, which we denote here as TLM_LR, to a higher rate one denoted here as TLM_HR, described in Table 3.

Plots of intermediary quantities generated with the OMSPA Software Receiver for the MarCO-B DOY 128 pass are shown in Figures 9 and 10, for TLM_LR and TLM_HR were in effect, respectively. In particular, the input sample PSD, the evolution of the recovered signal from samples to symbols,

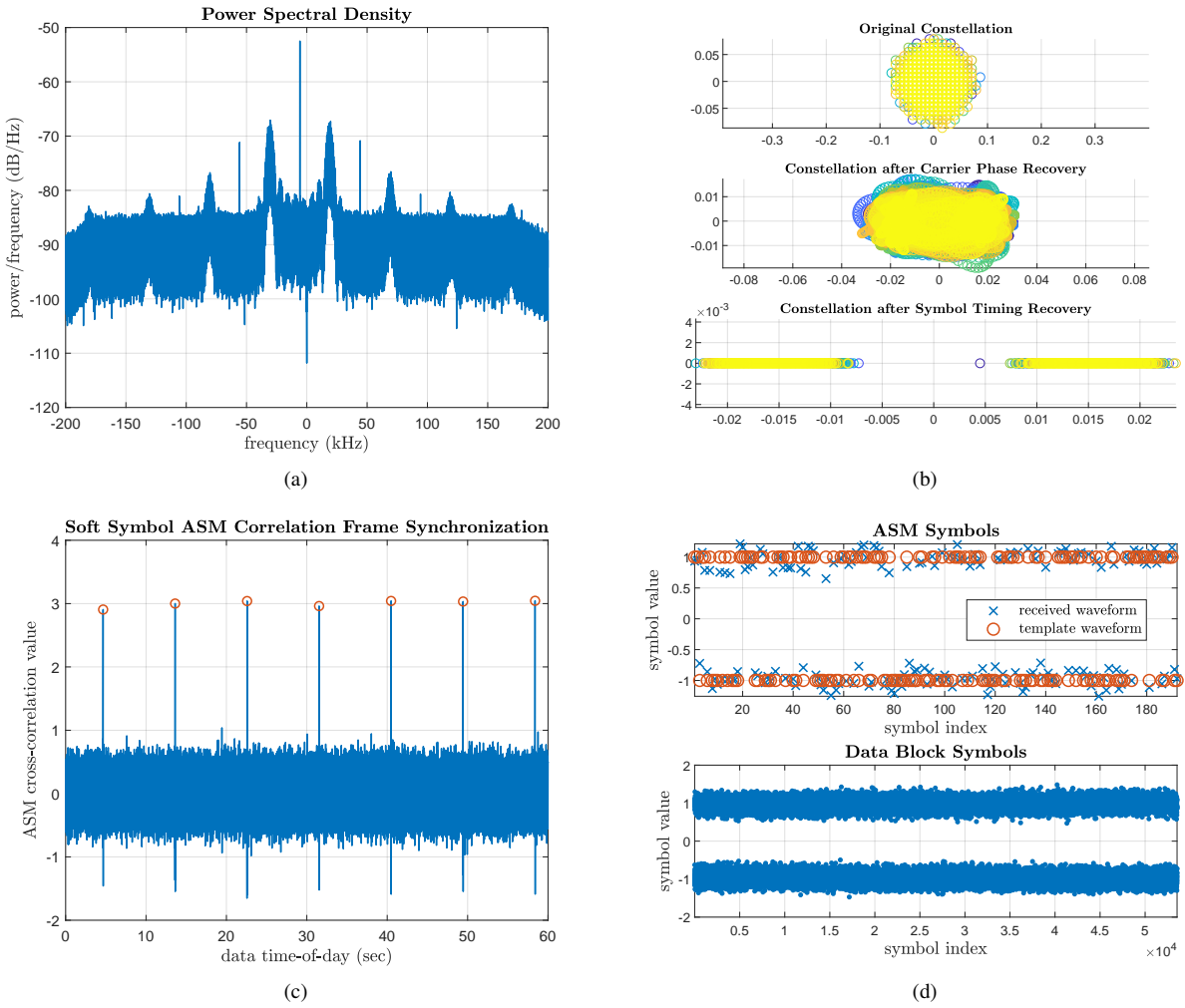


Figure 7. MarCO-A DOY 126 downlink demodulation result using the OMSPA Software Receiver: (a) input sample PSD, (b) evolution from samples to symbols via the Carrier Phase/Symbol Timing Recovery subsystems, (c) cross-correlation of output soft symbols with ASM sequence, (d) ASM/data symbols for one identified TF block.

	TLM_LR	TLM_HR
modulation type	PCM/PSK/PM; NRZ-L BPSK	PCM/PM; bi-phase-L BPSK
subcarrier	yes	no
coding	turbo	turbo
ASM bit pattern	25D5C0CE8990F6C9461BF79C DA2A3F31766F0936B9E40863	25D5C0CE8990F6C9461BF79C DA2A3F31766F0936B9E40863
TF length	8920	8920

Table 3. Settings for the MarCO lower rate TLM_LR and higher rate TLM_HR downlink telemetry modes.

the result of the cross-correlation of the output soft symbols with the ASM sequence, and the ASM/data symbols for one identified TF block are shown in (a), (b), (c), and (d), respectively, of Figures 9 and 10.

From the input sample PSD plots (Figure 9(a) and Figure 10(a)), the differences in the modes is evident, in that the subcarrier images present in the TLM_LR configuration are replaced with the wider bi-phase pulse shape in the TLM_HR configuration. Furthermore, as the symbol rate of

the TLM_HR mode is larger than that of the TLM_LR mode, the TLM_HR symbols effectively see more noise than the TLM_LR symbols do. This can be seen most prominently in the data block symbols of the synchronized TF shown in Figure 9(d) for TLM_LR and Figure 10(d) for TLM_HR.

Processing through the MarCO-B passes, the following results were found:

- DOY 126: 128 TFs recovered, all passed CRC except for 14 TFs,
- DOY 128:
 - TLM_LR: 46 TFs recovered, all passed CRC except for one TF (the 4th one),
 - TLM_HR: 504 TFs recovered, all passed CRC.

6. VALIDATION OF INSIGHT/MARCO RECOVERED TRANSFER FRAMES AGAINST DSN RECORDS

Recovered TFs extracted from the MSU InSight/MarCO launch window data sets were validated against those obtained from the DSN. Furthermore, a self-consistency type

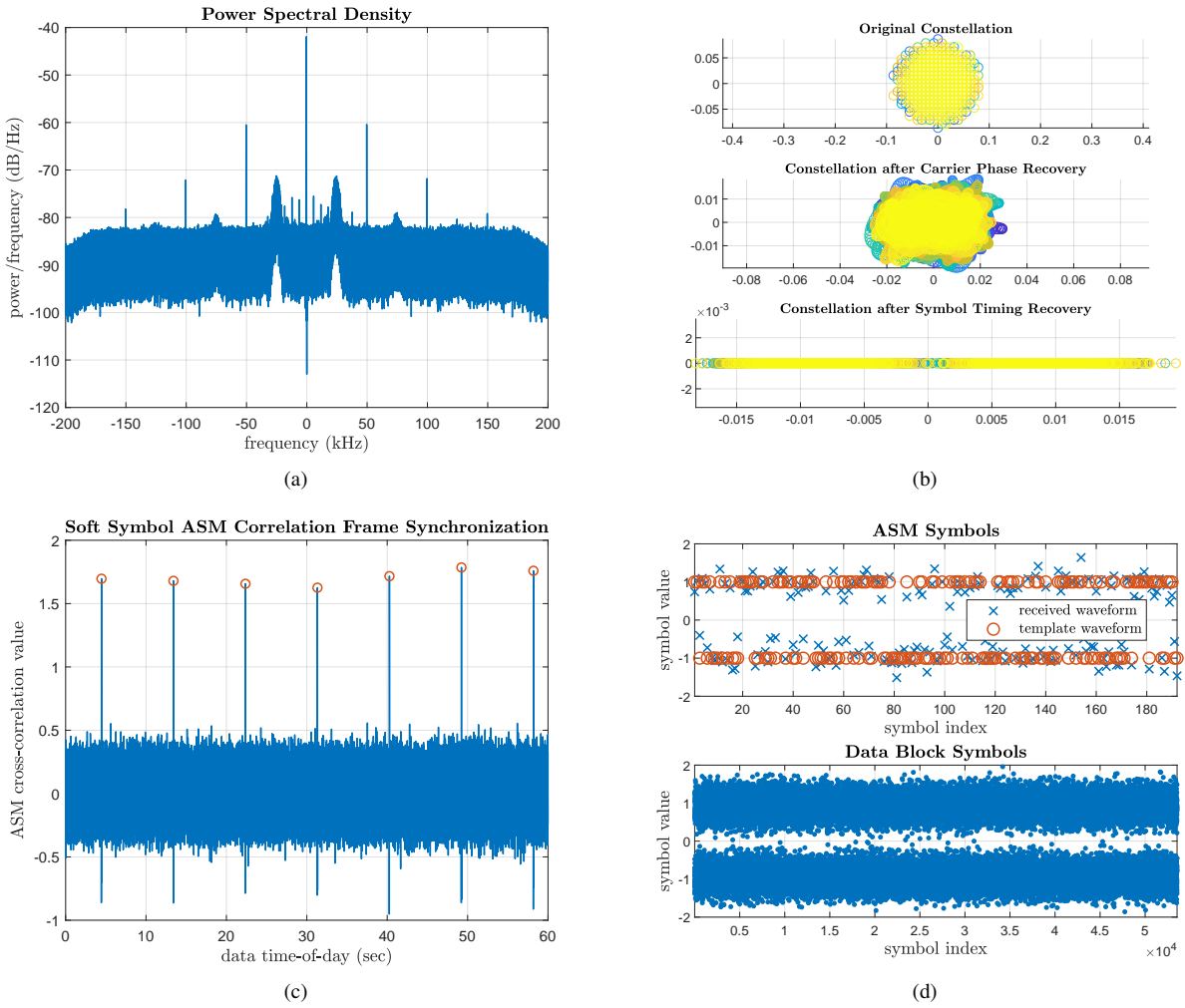


Figure 8. MarCO-A DOY 128 downlink demodulation result using the OMSPA Software Receiver: (a) input sample PSD, (b) evolution from samples to symbols via the Carrier Phase/Symbol Timing Recovery subsystems, (c) cross-correlation of output soft symbols with ASM sequence, (d) ASM/data symbols for one identified frame block.

validation was carried out with respect to the OMSPA Software Receiver using wideband very long baseline science receiver (WVSR) data collected at Deep Space Station (DSS) 26 at the Goldstone Deep Space Communications Complex (GDSCC). Specifically, WVSR data was only collected on DOY 128 over the following epochs:

- InSight:
 - Start time: 2018, DOY 128, 14:50:01 UTC,
 - End time: 2018, DOY 128, 14:50:01 UTC;
- MarCO-A:
 - Start time: 2018, DOY 128, 14:50:04 UTC,
 - End time: 2018, DOY 128, 14:50:04 UTC;
- MarCO-B:
 - Start time: 2018, DOY 128, 14:50:04 UTC,
 - End time: 2018, DOY 128, 14:50:04 UTC.

The following DSN data was available here for validation of the InSight/MarCO launch window OMSPA demonstration:

- InSight:
 - DOY 126 (DSS 34, 74), DOY 129 (DSS 24, 35, 74, 84);
- MarCO-A/B:
 - DOY 126, 128, 129 (TFs synthesized from all DSS

antennas).

From this, along with the recording epochs captured at MSU described in Section 5, it can be seen that the only possible validation opportunities were as follows:

- InSight: DOY 126 (MSU only),
- MarCO-A/B: DOY 126 (MSU only), DOY 128 (MSU and WVSR).

In the sequel, validation rate here refers to the percentage of all possible MSU/WVSR TFs passing CRC that can align with a set of DSN TFs that actually have a match with those TFs.

InSight DOY 126 Validation Results

Recall from above that DSN data for InSight on DOY 126 was collected at DSS 34, located at the Canberra Deep Space Communication Complex (CDSCC), and DSS 74, located at the University of Chile, Santiago Satellite Tracking Station. Unfortunately, when InSight was visible from MSU on DOY 126, it was not visible from either DSS 34 or DSS 74. In other words, when InSight was transmitting downlink on DOY 126, the data collected from MSU, as well as that captured from

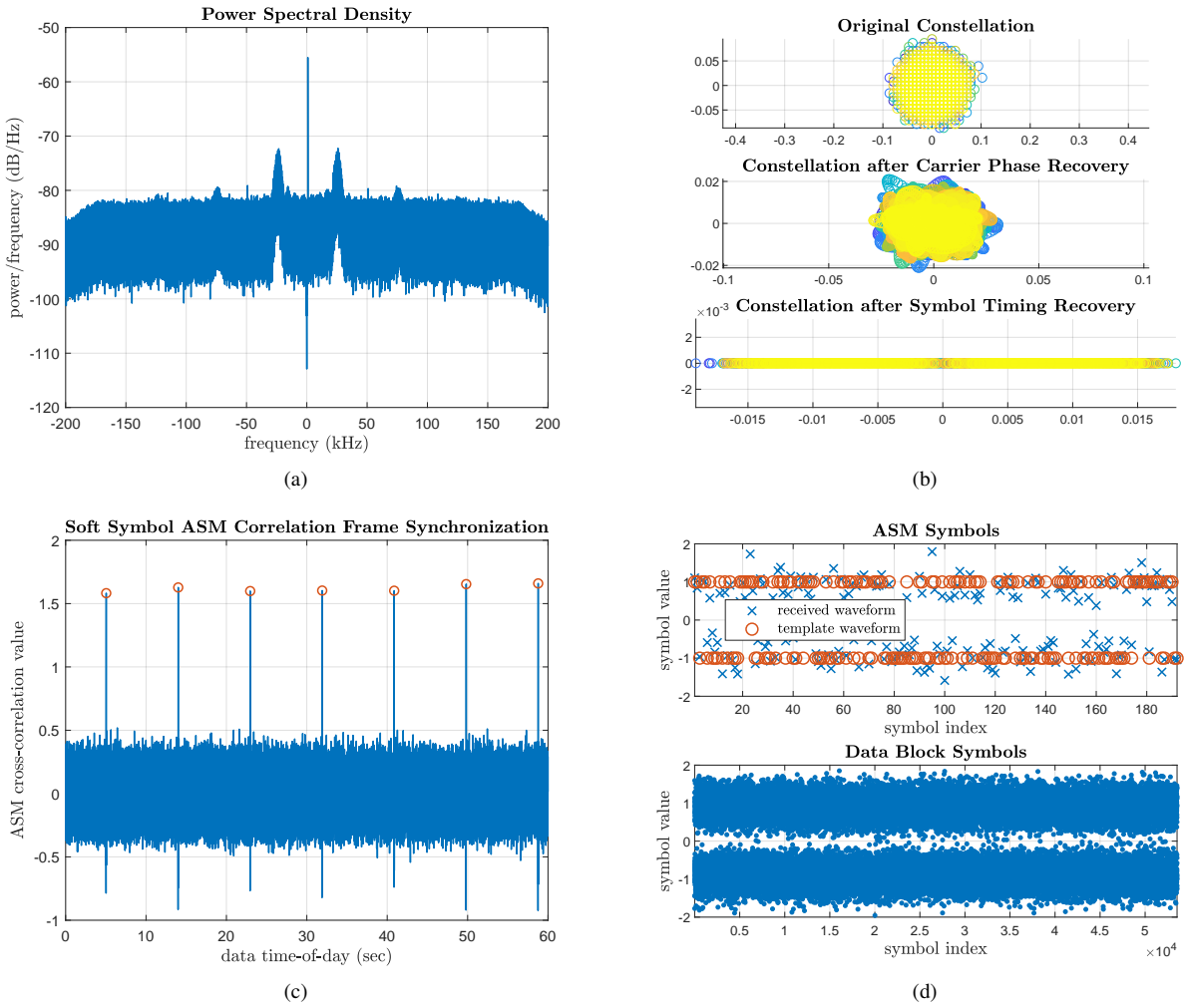


Figure 9. MarCO-B DOY 128 TLM_LR downlink demodulation result using the OMSPA Software Receiver: (a) input sample PSD, (b) evolution from samples to symbols via the Carrier Phase/Symbol Timing Recovery subsystems, (c) cross-correlation of output soft symbols with ASM sequence, (d) ASM/data symbols for one identified frame block.

the DSN (at DSS 34, 74), corresponded to non-overlapping periods of time. As such, no validation could be carried out for InSight on DOY 126.

MarCO-A DOY 126 Validation Results

The validation results for the MarCO-A DOY 126 data sets are shown in Table 4. As can be seen here, the MSU record preceded that of the DSN, leading to 69 TFs recovered by MSU that were not captured by the DSN. Furthermore, it appears as though one TF dropped by the DSN was picked up by MSU. This was ascertained by analyzing the Earth Received Time (ERT) of the DSN TFs. As desired, the validation rate for this pass was 100%.

MarCO-A DOY 128 Validation Results

The validation results for the MarCO-A DOY 128 data sets are shown in Table 5. Here, the exact matches between DSN TFs 1:181 and MSU TFs 7:187 corresponded only to those MSU TFs which passed CRC. Also, both the WVSR and MSU records preceded that of the DSN, leading to 25 TFs recovered by WVSR and 6 TFs recovered by MSU that were not captured by the DSN. As desired, the validation rate for this pass was 100% for both the WVSR and MSU records,

with respect to the DSN record.

MarCO-B DOY 126 Validation Results

The validation results for the MarCO-B DOY 126 data sets are shown in Table 4. Here, the exact matches between DSN TFs 66:100 and MSU TFs 1:35, as well as between DSN TFs 101:193 and MSU TFs 37:128, corresponded only to those MSU TFs which passed CRC. Also, it appears as though one TF dropped by the DSN was picked up by MSU, as determined through an ERT analysis of the DSN TFs. As desired, the validation rate for this pass was 100%.

MarCO-B DOY 128 Validation Results

Recall from Section 5 that this pass was unique in that the telemetry modes changed from TLM_LR to TLM_HR partway through the pass (see Table 3 for more information about these modes). The validation results for the MarCO-B DOY 128 data sets are shown in Table 7. From this, it can be seen that the DSN recovered frames only consisted of TLM_HR data, and furthermore, the entire MSU data precedes the start of the DSN TF data record. As such, validation of the MSU data could only be made with respect to the WVSR data. Since the WVSR data encompasses a time

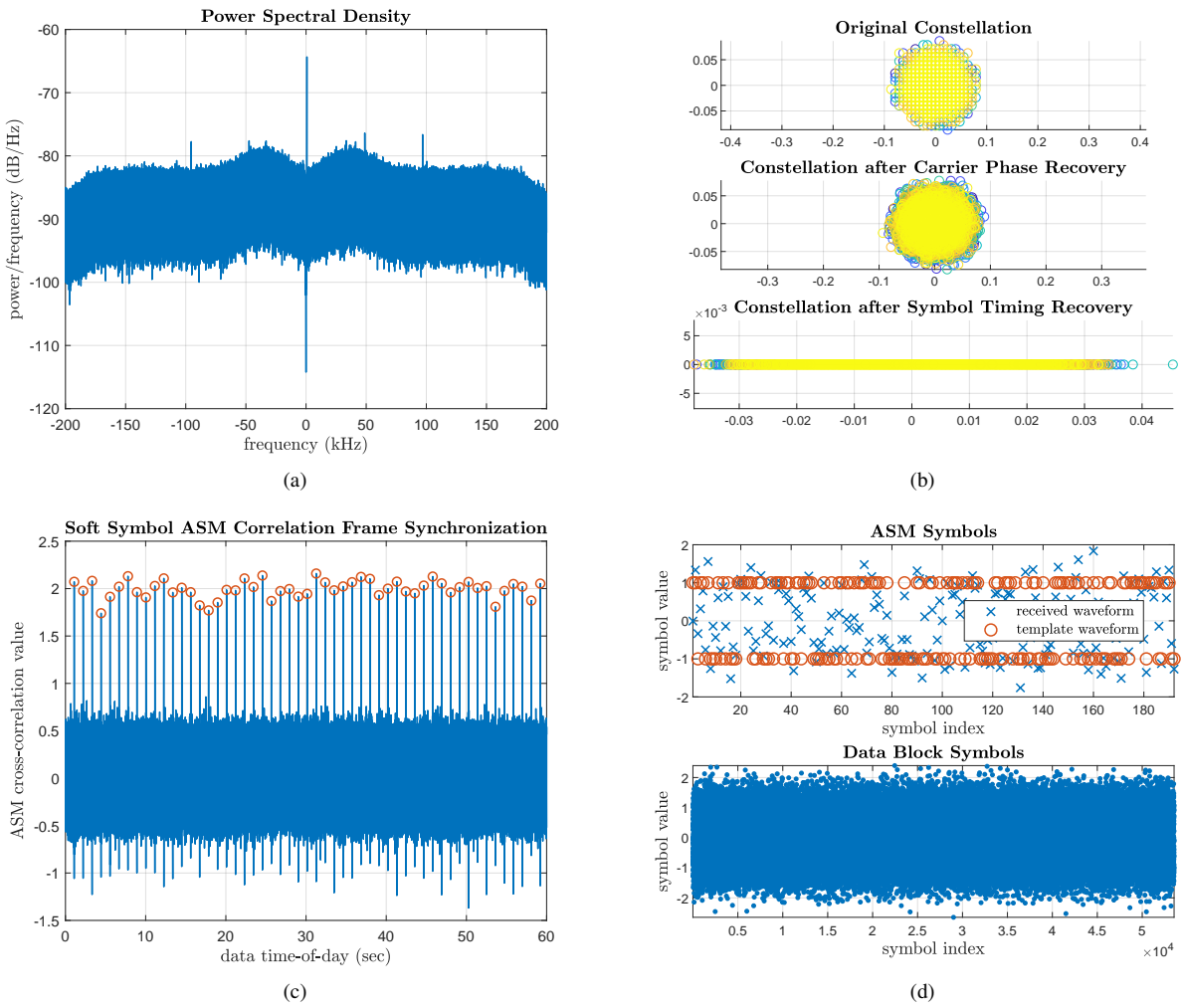


Figure 10. MarCO-B DOY 128 TLM_HR downlink demodulation result using the OMSPA Software Receiver: (a) input sample PSD, (b) evolution from samples to symbols via the Carrier Phase/Symbol Timing Recovery subsystems, (c) cross-correlation of output soft symbols with ASM sequence, (d) ASM/data symbols for one identified frame block.

MarCO-A 2018 DOY 126 Validation Results		
	DSN	MSU
total # of TFs recovered	571	187
TFs failing CRC	none	none
total # of TFs passing CRC	571	187
exact matches	1:69	70:138
	70:117	140:187
comments	<ul style="list-style-type: none"> MSU TFs 1:69 precede start of DSN TF data record, ERT analysis of DSN data suggests that exactly one TF is missing between DSN TF 69 and 70, which appears to be filled in by MSU TF 139. 	
validation rate	100%	

Table 4. Validation results for the MarCO-A 2018 DOY 126 DSN/MSU data sets.

period that includes both the DSN and MSU records, it serves as a bridge to link the DSN and MSU records.

As with the previous validation results, the exact matches between the TLM_LR WWSR TFs 17:62 and TLM_LR MSU

TFs 1:46 corresponded only to those MSU TFs which passed CRC (i.e., all TLM_LR MSU TFs except for TF 4). Regarding TLM_LR data, there was a TF in the WWSR data that was not picked up by the MSU data. Also, the latter TLM_LR data from WWSR matched that of the beginning TFs captured

MarCO-A 2018 DOY 128 Validation Results			
	DSN	WVSR	MSU
total # of TFs recovered	542	206	187
TFs failing CRC	none	none	13-18, 21-25, 27, 28, 31, 45
total # of TFs passing CRC	542	206	172
exact matches	1:181	26:206	7:187
comments	<ul style="list-style-type: none"> WVSR TFs 1:25 and MSU TFs 1:6 precede start of DSN TF data record. 		
validation rate	100% (WVSR), 100% (MSU)		

Table 5. Validation results for the MarCO-A 2018 DOY 128 DSN/WVSR/MSU data sets.

MarCO-B 2018 DOY 126 Validation Results		
	DSN	MSU
total # of TFs recovered	393	128
TFs failing CRC	none	30, 40, 50, 86-92, 99, 115, 119, 121
total # of TFs passing CRC	393	114
exact matches	66:100	1:35
	101:193	37:128
comments	<ul style="list-style-type: none"> ERT analysis of DSN data suggests exactly one TF is missing between DSN TF 100 and 101, which appears to be filled in by MSU TF 36. 	
validation rate	100%	

Table 6. Validation results for the MarCO-B 2018 DOY 126 DSN/MSU data sets.

MarCO-B 2018 DOY 128 Validation Results			
	DSN	WVSR	MSU
total # of TFs recovered	(TLM_LR): none (TLM_HR): 1024	(TLM_LR): 62 (TLM_HR): 1105	(TLM_LR): 46 (TLM_HR): 504
TFs failing CRC	(TLM_LR): none (TLM_HR): none	(TLM_LR): none (TLM_HR): none	(TLM_LR): 4 (TLM_HR): none
total # of TFs passing CRC	(TLM_LR): none (TLM_HR): 1024	(TLM_LR): 62 (TLM_HR): 1105	(TLM_LR): 45 (TLM_HR): 504
exact matches		(TLM_LR): 17:62	(TLM_LR): 1:46
		(TLM_HR): 2:505	(TLM_HR): 1:504
	(TLM_HR): 1:507	(TLM_HR): 599:1105	
comments	<ul style="list-style-type: none"> WVSR TLM_LR TFs 1:16 precede the start of the MSU TLM_LR data, WVSR TLM_HR TF 1 precedes the start of the MSU TLM_HR data, Entire MSU data precedes start of the DSN TF data record, WVSR TLM_HR TFs 1:598 precede the start of the DSN TF data record. 		
validation rate	100% (WVSR & DSN), 100% (MSU & WVSR)		

Table 7. Validation results for the MarCO-B 2018 DOY 128 DSN/WVSR/MSU data sets.

by the DSN. As desired, the validation rate for this pass was 100% for both the WVSR data, with respect to the DSN data, as well as for the MSU data, with respect to the WVSR data.

7. CONCLUSION

In this article, we demonstrated the demodulation capabilities of the MATLAB-based OMSPA Signal Processing Software Receiver with regards to the InSight/MarCO launch window. Specifically, it was shown that CB samples of X-band downlink telemetry from InSight, MarCO-A, and MarCO-B, recorded simultaneously at MSU while tracking InSight using its 21-m antenna, could each be demodulated when MarCO-A and MarCO-B remained within the antenna main beam. Diagnostic outputs from the OMSPA Software Receiver showed the demodulation process in action, including carrier phase and symbol timing recovery, along with frame synchronization and decoding.

Power spectra from the MSU data captures were shown to be in line with intuition, in terms of relative position of the residual carrier, subcarrier positioning, and relative SNR with regards to link margin and symbol rate. Validation of the TFs recovered from the MSU data captures, with respect to those yielded by WVSR sample data and DSN TF data records, showed perfect agreement for all potential match candidate TFs that passed CRC.

The results of this demodulation effort highlight the possibility of future use of the OMSPA Software Receiver in expanding the capabilities of the DSN. In particular, efforts have been underway at JPL to chart a path toward infusion of the OMSPA concept in the DSN. The prime objective of this task has been to identify a method of incorporating the entire OMSPA system with minimal to no impact on current DSN operations. A breakdown of the subsystems required for such an OMSPA infusion method are as follows:

- OMSPA Service Management: (subsystem consisting of two components: OMSPA Portal and OMSPA Service Manager)
 - OMSPA Portal:
 - * Interface through which external customers can request an OMSPA opportunity search and receive a set of output products from demodulated passes, including TFs, one-way Doppler estimates, and QoS reports for the passes.
 - OMSPA Service Manager:
 - * Module that passes information back and forth between the OMSPA Portal and subsystems internal to the DSN;
 - * Calculates OMSPA opportunities based on receive antenna positioning, spacecraft ephemeris files, and downlink telemetry capture windows;
 - * Triggers recording sessions on the DSN Open Loop Receiver (OLR) hardware;
 - * Generates OMSPA Software Receiver instantiations as virtual machines (VMs) on one rack unit (1U) of existing DSN hardware;
 - * Interfaces with the OLR, OMSPA Software Receiver, and OMSPA Portal to provide the required inputs/outputs.
- OMSPA Signal Processing: (subsystem consisting of OMSPA Software Receiver instantiations)
 - Takes in telemetry parameters from OMSPA Service Manager and reads in data recorded by the OLR;
 - Demodulates CB sample data provided by OLR and

returns a set of output products to the OMSPA Service Manager including the recovered TFs (formatted as in [9]), one-way Doppler estimates (expressed in Tracking Data Message (TDM) format [10]), and a QoS report of the pass data.

To the extent that such infusion occurs in the future, the DSN would be able to offer the smallsat community a reliable, low-cost beam-sharing service in which the smallsats do not have to always compete for downlink antenna time. Instead, they could make use of DSN antennas that have already been scheduled by other spacecraft, when in beam with them. That the OMSPA technique was also successfully demonstrated on the MSU 21-m antenna using readily available, low-cost software-defined radios (SDRs) and computers suggests that OMSPA could be applied to just about any dish antenna equipped with an appropriate IF feed from which a recording can be made.

ACKNOWLEDGMENTS

The authors would like to thank MSU's Jeff Kruth and Robert Kroll for their technical consultation and assistance in establishing and testing MSU's recording capabilities; the MarCO Chief Engineer's (Andy Klesh's) assistance in validating the OMSPA-recovered data for MarCO; InSight's Sanford Krasner and Kris Bruvold for their assistance in validating the OMSPA-recovered data for InSight; and, the DSN Mission Interface Managers (MIMs), Serjic Zadourian and Freia Weisner, for their help arranging data validation with MarCO and InSight, respectively.

REFERENCES

- [1] D. S. Abraham, S. G. Finley, D. P. Heckman, N. E. Lay, C. M. Lush, and B. E. MacNeal, "Opportunistic MSPA Demonstration #1: Final Report," *Interplanetary Network Progress Report*, vol. 42-200, pp. 1-27, February 15, 2015.
- [2] N. Lay, M. Lyubarev, A. Tkacenko, M. Srinivasan, K. Andrews, S. Finley, C. Goodhart, and R. Navarro, "Software Receiver Processing for Deep Space Telemetry Applications," *Interplanetary Network Progress Report*, vol. 42-180, pp. 1-8, February 15, 2010.
- [3] *TM Synchronization and Channel Coding*, Blue Book, Consultative Committee for Space Data Systems (CCSDS) Recommendation for Space Data System Standards CCSDS 131.0-B-3, Sep. 2017. [Online]. Available: <https://public.ccsds.org/Pubs/131x0b3e1.pdf>
- [4] J. G. Proakis and M. Salehi, *Digital Communications*, 5th ed. New York, NY: McGraw-Hill Education, Nov. 2007.
- [5] F. J. Harris, *Multirate Signal Processing for Communication Systems*. Upper Saddle River, NJ: Prentice Hall PTR, May 2004.
- [6] M. M. Shihabi, T. M. Nguyen, and S. M. Hinedi, "A comparison of telemetry signals in the presence and absence of a subcarrier," *IEEE Trans. Electromagn. Compat.*, vol. 36, no. 1, pp. 60-73, Feb. 1994.
- [7] *TM Synchronization and Channel Coding - Summary of Concept and Rationale*, Green Book, Consultative Committee for Space Data Systems (CCSDS) Recommendation for Space Data System Standards CCSDS 130.1-G-2, Nov. 2012. [Online]. Available: <https://public.ccsds.org/pubs/130x1g2.pdf>

- [8] J. Hamkins and M. K. Simon, Ed., *Autonomous Software-Defined Radio Receivers for Deep Space Applications*, Deep Space Communications and Navigation Series. Jet Propulsion Laboratory, California Institute of Technology, 2006, vol. 9.
- [9] *0161-Telecomm Telemetry Standard Formatted Data Unit (SFDU) Interface*, Deep Space Network, 820-013, JPL D-76513, 0161-Telecomm, Revision B, Sep. 2014.
- [10] *0212-Tracking Tracking Data Message (TDM) Interface*, Deep Space Network, 820-013, JPL D-16765, 0212-Tracking-TDM, Revision D, Oct. 2015.

BIOGRAPHY



Andre Tkacenko received his B.S., M.S., and Ph.D. degrees in Electrical Engineering from the California Institute of Technology in 1999, 2001, and 2004, respectively. Since 2005, he has been with the Jet Propulsion Laboratory, where he is currently a signal analysis engineer in the Signal Processing And Networks Group (332C). His current work focus is in spectrum management,

deep space optical communications, and software receiver design.



Zaid Towfic holds a B.S. in Electrical Engineering, Computer Science and Mathematics from the University of Iowa. He received his Electrical Engineering M.S. in 2009 and Ph.D. in 2014, both from UCLA, where he focused on signal processing, machine learning, and stochastic optimization. After receiving his Ph. D., Zaid joined the MIT Lincoln Laboratory where he

worked on distributed beam forming and geolocation, interference excision via subspace methods, simultaneous communication, and electronic warfare. Zaid joined the Jet Propulsion Laboratory in January of 2017 and has been focused on machine learning and signal processing efforts.



Murphy Stratton received her B.S. in Space Science and her M.S. in Space Systems Engineering from Morehead State University in 2016 and 2018, respectively. While at Morehead State, Murphy focused mainly on systems engineering, RF engineering, and ground station architecture. She worked closely with NASA JPL on the OMSPA project and demonstration. After receiving her

Masters, Murphy began a career at the University of Illinois of Urbana-Champaign as the Laboratory Manager for the CubeSat Laboratory in the Aerospace Engineering department. She also works as a project manager for flight projects at UIUC and contributes to proposals for future flight projects.



Doug Abraham is a Senior Systems Engineer within the Jet Propulsion Laboratory's Interplanetary Network Directorate (IND), which manages the Deep Space Network (DSN) and the Advanced Multi-Mission Operations System (AMMOS). For the past 20 years, Doug has served in a variety of DSN-related capacities, most recently serving as IND's Strategic and Systems Forecasting Lead.

Prior to that, Doug spent 10 years working within JPL's Mission and Systems Architecture Section, supporting the Galileo, Ulysses, and Cassini missions, as well as the Pluto Fast Flyby and "Ice and Fire" pre-formulation activities. He began his career in Reston, Virginia as a graduate student intern within the International Space Station's Program Requirements & Assessment Office. Doug graduated Magna Cum Laude from Texas A&M University in Physics (1986) and earned an M.S. in Technology and Science Policy, with specialization in technology assessment and electrical engineering, from Georgia Tech (1990).



Sue Finley has been an employee of NASA's Jet Propulsion Laboratory (JPL) since January 1958, making her the longest-serving woman in NASA. Two days before Explorer 1 was launched, Finley began her career with the laboratory as a human computer, calculating rocket launch trajectories by hand. She now serves as a subsystem engineer for NASA's Deep Space Network (DSN). At

JPL, she has participated in the exploration of the Moon, the Sun, all the planets, and other bodies in the Solar System.



Shan Malhotra is a Principal Engineer at NASA's Jet Propulsion Lab. He focuses on building mission critical ground data systems. For the past 20 years he has worked as a System Engineer on DSN's Service Management System – which is responsible for prediction and configuration of the systems as part of realtime tracking. In the last 10 years he has worked as the System Engineer

for the Treks – a series of Graphical Information Systems that support planetary science, mission design and public outreach for the Moon, Mars, Vesta, Titan and even Earth.

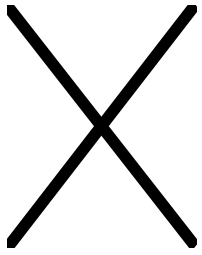


Andrew O'Dea received his ...

Benjamin K. Malphrus is Director of the Morehead State University Space Science Center. He serves as project director for the 21 M Space Tracking Antenna (Deep Space Station 17) operated by the Center. He has served on the scientific staff of the National Radio Astronomy Observatory, and as visiting scientist at NASA's Wallops Flight Facility. He has served as PI or co-PI on several

nanosatellite missions including Lunar IceCube, KySat-2, the Cosmic X-Ray Background Nanosatellite, CXBN-2, and TechSat-1. He has published papers in scientific journals on topics ranging from extragalactic astrophysics to instrumentation in radio astronomy, to space systems engineering. Dr. Malphrus served as PI on over \$20 million R&D grant

funding and led the design of a \$16 million R&D center for space sciences. In the 1990s, he led a team that developed a theory of galaxy formation that has gained wide acceptance among the astronomical community.



Chuck Conner received his ...